Discovery of new polymorphs of gallium oxides with particle swarm optimization based structure searches

Xue Wang,[1,†] Muhammad Faizan,[1,†] Guangren Na,[1] Xin He,[1] YuHao Fu,[,2] and Lijun Zhang[*,1]*

[1]State Key Laboratory of Integrated Optoelectronics, Key Laboratory of Automobile Materials of MOE and College of Materials Science and Engineering, Jilin University, Changchun 130012, China

[2]College of Physics, Jilin University, Changchun 130012, China

[†]These authors contributed equally

*E-mail: fuyuhaoy@gmail.com; lijun_zhang@jlu.edu.cn

Gallium Oxide (Ga_2O_3) has attracted significant research interest for next-generation high-efficiency power devices because of their unique electronic properties such as ultra-wide band gap, high breakdown electric field, and large Baliga's figure of merit. Ga_2O_3 crystallizes in a series of reported polymorphs including β-, α-, ε-, κ-, γ- and δ-Ga_2O_3, the structures of some of which are still in serious controversy. We herein performed a polymorph structure search study of Ga_2O_3 by combining particle swarm optimization with first-principles energetic calculations. In addition to producing the predominant experimental known phases of β-, α- and κ-Ga_2O_3, we found two new polymorphs with space group $P\bar{1}$ and $Pmc2_1$ consisting of four- and five-fold coordinated Ga. They show comparable energy with β- and α-Ga_2O_3 with the energy difference of several meV/atom, and exhibit robust phonon stability. Similarly, the new phases show quite wide band gaps and small electron effective masses by comparing it with other known phases. The $Pmc2_1$ phase shows a calculated spontaneous polarization of 0.277 C/m^2, close to that of ε/κ-Ga_2O_3. Our systemic structure searches also establish a structural relationship between ε-Ga_2O_3 and κ-Ga_2O_3 and how the electronic properties vary with polymorphic phase change.

1. Introduction

Recently wide-bandgap semiconductors (WBGSs) are becoming increasingly important in high-power devices.[1–3] They permit electronic devices to operate at much higher voltages, frequencies, temperatures and radioresistance than conventional semiconductors, like Si and GaAs.[4] Gallium oxide (Ga_2O_3) is one of the WBGSs that has ultra-large band gap (E_g) of ~4.8-5.1 eV and optimum Baliga's figure of merits (BFOM).[5–12] The band gap of Ga_2O_3 is smaller than that of diamond having the largest value of ≈5.47 eV in the semiconductor family.[13,14] It may exist in different polymorphic forms including α-, β-, ε-, γ-, κ-, and δ-Ga_2O_3 phases, among which β-Ga_2O_3 (*C*2/*m*) is the most studied polymorphic model due to its high thermodynamic stability, easy preparation, and superior performance in high power electronic devices, i.e. field-effect transistor.[13,15–21]

In each designated Ga_2O_3 polymorphs, oxygen atoms form the same close packing environment, whereas Ga atoms occupy octahedral and tetrahedral positions with different proportions.[22] β-Ga_2O_3 polymorph contains equal proportions of Ga^{3+} (with 1:1 ratio) in octahedral and tetrahedral sites.[23] It is the most stable phase amid the reported Ga_2O_3 polymorphs. α-Ga_2O_3 polymorph contains only octahedrally coordinated Ga and is found similar to the hexagonal α-Al_2O_3 ($R\bar{3}c$).[24] α-Ga_2O_3 polymorph is a metastable phase and transforms into β-Ga_2O_3 under ambient pressure over ≈650 ℃. Currently, there are some controversies in the literature concerning the exact crystal structure of γ-Ga_2O_3. This phase is speculated to be a defect spinel structure ($Fd\bar{3}m$), analogous to γ-Al_2O_3 and η-Al_2O_3.[25] On the other hand, the pair distribution function investigation reveals space group of γ-Ga_2O_3 is $F4\bar{3}m$. Similarly, the crystal structure of ε-Ga_2O_3 also faces some controversy. Initial XRD measurements confirm $P6_3mc$ structure containing Ga both at the octahedral and tetrahedral sites. The structure is found similar to ε-Fe_2O_3 and κ-Al_2O_3.[22,26–30] However, TEM measurement shows Ga and their vacancies retain ordering with (110)-twined domains. The domain possesses an orthorhombic phase with space group $Pna2_1$ referred to as κ-Ga_2O_3.[31] The ε-Ga_2O_3 polymorph is considered as the

most stable form of Ga_2O_3 after β-Ga_2O_3.[29,30] δ-Ga_2O_3 is an analogue of bixbyite as indicated for In_2O_3.[24] The novel κ-Ga_2O_3 possesses orthorhombic structure (*Pna*2_1) with tetrahedral/octahedral coordinated Ga ratio of 1:3.[26] It is formed due to the thermal decomposition of $Ga_5O_7(OH)$ before transforming to β-Ga_2O_3.[26]

Materials with large band gap often have large dielectric constant, which are highly beneficial for ferroelectricity. In a study reported by Kim and his co-workers, the calculated spontaneous polarization of κ- and ε-Ga_2O_3 reach ~26.39 (κ-Ga_2O_3@E_g=4.62 eV) and 24.44 (ε-Ga_2O_3@E_g=4.27 eV) μC/cm^2, respectively.[29] Subsequent experiments also confirmed the ferroelectricity of ε-Ga_2O_3 by digital holographic microscopy (DHM) technique.[30] Measurements specified by Pavesi et al. have shown that single phase ε-Ga_2O_3 possesses large dark resistivity and wide band gap ~4.6 eV and can be used as highly efficient materials for solar-blind UV photodetectors.[32]

In the present work, we performed a systematic structure search study of the gallium oxides Ga_2O_3 with first-principles particle swarm optimization (PSO) algorithm. We found two new metastable polymorphs of Ga_2O_3 with space group $P\bar{1}$ and *Pmc*2_1. The new phases contain unreported motifs with four- and five-fold coordinated Ga, possess ultra-wide band gaps, and favorable electron effective masses. In addition, the *Pmc*2_1 has a considerable spontaneous polarization (~0.28 C/m^2), implying a great promise for ferroelectric applications.

2. Computational Methods

Structure searching of Ga_2O_3 polymorphs was performed using the first-principles structure prediction method as implemented in the CALYPSO code.[33,34] More than 4800 structures were investigated during the Ga_2O_3 polymorphs search. The first-principles calculations of the total energy were performed using the plane-wave projector-augmented-wave (PAW) method[35] as implemented in the Vienna Ab initio simulation package (VASP).[36] The *4s*, *4p*, *3d* (Ga), and *2s*, *2p* (O) electrons were treated explicitly as valence electrons. We used the generalized gradient

approximation (GGA) of Perdew, Burke, and Ernzerhof (PBE) as the exchange-correlation functional.[37] Structural optimizations were done with kinetic energy cutoff 520 eV and Monkhorst-Pack k-point meshes of spacing $2\pi\times0.03$ Å^{-1}. Electronic band structure calculations were carried out using the Heyd−Scuseria−Ernzerhof (HSE06) hybrid functional with 37% non-local Hartree Fock exchange, which ensures to match the experimental band gap of known α-, β- and κ-Ga_2O_3 polymorphs.[38–40]

Phonon dispersion calculations of the new phases ($P\bar{1}$ and $Pmc2_1$) were conducted using the real-space supercell method as implemented in the Phonopy package.[41,42] The electron and hole effective masses (m_e* and m_h*) were obtained with BoltzTraP code.[43] We calculated the spontaneous polarization of κ-Ga_2O_3 and $Pmc2_1$ using the Berry phase approach.[44–46] Consideration of similar structures can interfere with data analysis, we, therefore, adopted bond characterization matrix (BCM) method[47] to eliminate similar structures from the structure searching and left only ~800 structures to explore the relationship amid the energy, band gap, and coordination numbers (CNs) of Ga_2O_3 polymorphs.

3. Results and Discussion

3.1. Searching Ga_2O_3 Polymorphs through Particle Swarm Optimization

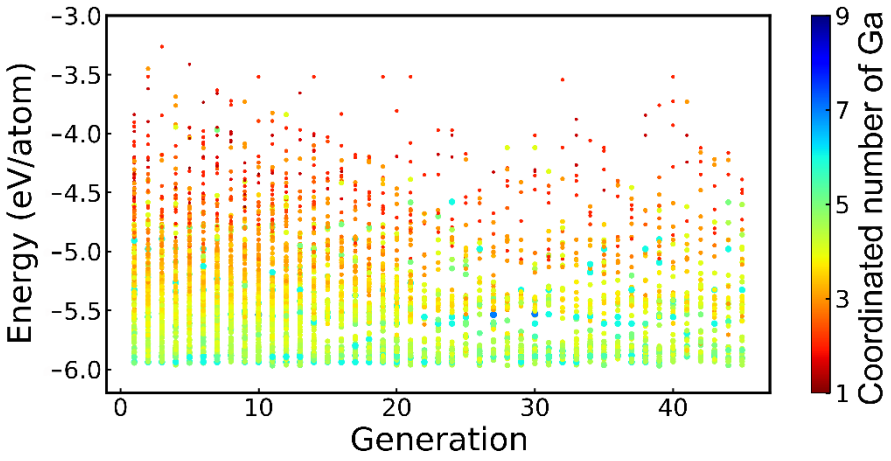

Figure 1. The energy versus generation for different Ga_2O_3 polymorphs. The colored circles display the averaged coordination number of Ga.

Structure search studies that involve total energy minimization of thousands of candidate structures are very expensive in the computational cost. It is especially time consuming for the unit cells with the large number of formulas. Therefore, usually the fixed number of formulas have to be assumed in the unit cells. It is known that for the synthesized Ga_2O_3 polymorphs, the unit cells contain 2 or 8 formulas (*e.g.*, 2 for β-Ga_2O_3 and 8 for κ-Ga_2O_3). We thus first performed our structure searches with 2 and 8 formulas in unit cells. To test the convergence of structure searching, we carried out additional new structure searches with 3-, 4- and 6-formula in unit cells. However, the lowest-energy structure from the additional structure searches is still ~0.017 eV/atom higher than the experimentally known phase with the highest energy, α-Ga_2O_3. This implies that our structure searches with two and eight formulas have reached convergence. Throughout these calculations, we explored more than 4800 structures in the free energy potential landscape of Ga_2O_3. Figure 1 presents total energies as a function of generation for the structure searching of Ga_2O_3 polymorphs. We found that most of the structures in the low-energy range are the most stable β-Ga_2O_3 and metastable α-Ga_2O_3, where the averaged CNs of Ga are 5 and 6, respectively. κ-Ga_2O_3 polymorph is also predicted successfully corresponding to an averaged CNs of 5.5. In addition to the above findings, we surprisingly found two new metastable phases of Ga_2O_3 with space group $P\bar{1}$ and $Pmc2_1$. The new phases have somewhat high CNs. By sorting out the calculated energies, we found that E(β-Ga_2O_3) < E($P\bar{1}$) < E(κ-Ga_2O_3) < E($Pmc2_1$) < E(α-Ga_2O_3) (See Figure 2). The energy of the $P\bar{1}$ phase is close to β-Ga_2O_3 phase, only 3 meV/atom higher than this, while the energy of the $Pmc2_1$ phase lies between κ-Ga_2O_3 and α-Ga_2O_3. Additionally, we investigated the thermodynamic stability of the five phases. The calculated formation enthalpies are enlisted in Table S1 of the Supporting Information. The formation enthalpy of Ga_2O_3 can be written as $\Delta H(Ga_2O_3) = [E(Ga_2O_3) - 2E(Ga) - 3E(O)]$. We found that the formation enthalpies of two new phases are higher than the most stable β-Ga_2O_3, but lower than α-Ga_2O_3. The α-Ga_2O_3 has been synthesized in experiment and fabricated into devices. Considering the significant structure difference between the β-Ga_2O_3/α-Ga_2O_3 phases and the new phases, the transition barrier would be high. This implies that the predicted new phases ($P\bar{1}$ and $Pmc2_1$) are likely to be synthesized and tested experimentally.

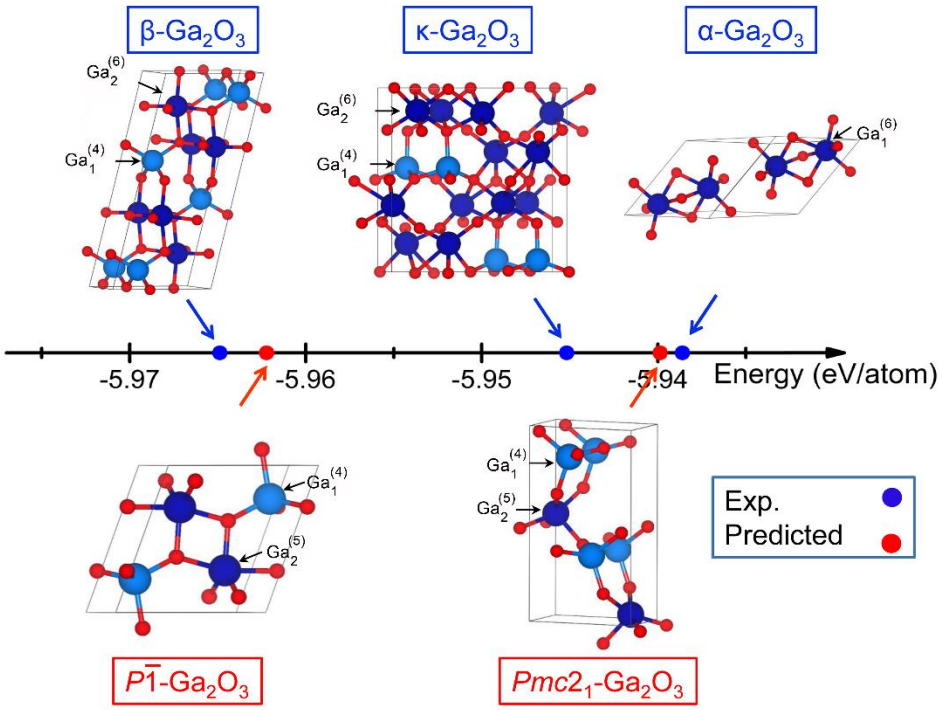

Figure 2. The low energy structures of β-, α-, κ-, $P\bar{1}$-, and $Pmc2_1$-Ga_2O_3 polymorphs. The blue and red spheres on the axis denote Ga and O atoms. The subscript shows the type of Ga whereas the superscript indicates the coordination number of Ga for Ga_2O_3 polymorphs.

To further distinguish the new phases from already known experimental structures, we simulated the XRD patterns using our in-house developed code and plotted the obtained results in Figure 3. By comparing with the experimental powder diffraction data of β- and α-Ga_2O_3, we found that all the calculated peaks show blue shifts owing to the slightly larger lattice parameters than experiments (See Table S2 of the Supporting Information). The calculated XRD patterns of $P\bar{1}$ and $Pmc2_1$ exhibit some remarkable diffraction peaks in the range from 10° to 70° compared with their other counterparts. The detailed lattice parameters are presented in Table S3 of the Supporting Information. Surprisingly, we found that the new phases include the novel motifs with 4- and 5-coordinated Ga. In the $P\bar{1}$ phase, Ga occupies two nonequivalent sites: Ga1 coordinated with four O neighbors forming a tetrahedron, and Ga2 located at the hexahedral sites surrounding five O atoms. In the $Pmc2_1$ phase, Ga also occupies Ga1 and Ga2 sites. Ga1 is located at the center of a tetrahedron with four nearest neighbors and Ga2 with five O neighbors formed a twisted pentahedron (See

Figure 2). The $P\bar{1}$ and $Pmc2_1$ phases have relatively small averaged bond lengths of Ga-O (1.919Å@$P\bar{1}$; 1.896Å@$Pmc2_1$) compared with three known phases (1.966Å@β-Ga_2O_3; 2.031Å@α-Ga_2O_3; 2.013Å@κ-Ga_2O_3) as listed in Table S4 of the Supporting Information.

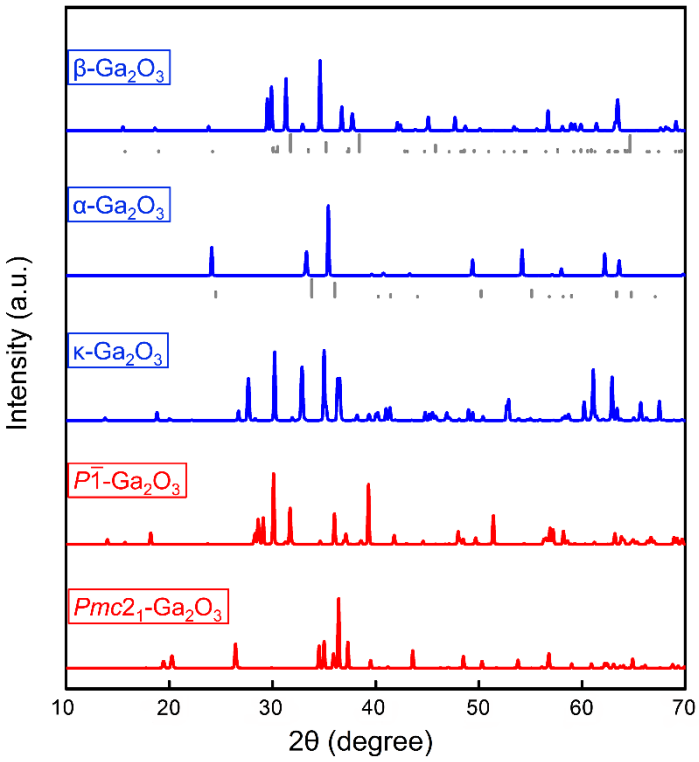

Figure 3. X-ray diffraction (XRD) patterns of the β-Ga_2O_3, α-Ga_2O_3, κ-Ga_2O_3, $P\bar{1}$- Ga_2O_3, and $Pmc2_1$-Ga_2O_3 simulated with Cu $K\alpha 1$ radiation. The blue curves represent the experimental structures while the red curves show the predicted structures. Experimental XRD patterns of β-Ga_2O_3 and α-Ga_2O_3 are represented by the grey lines for comparison.

3.2. Phonon Spectra and Electronic Properties of $P\bar{1}$- and $Pmc2_1$-Ga_2O_3

The calculated phonon dispersion spectra of the new phases are plotted in Figure 4(a, b). No imaginary phonon frequencies are found in the whole Brillouin zone, indicating that they are dynamically stable. It is noticed that the low-frequency optical phonons at Y symmetry point show a softening trend in the $Pmc2_1$ phase, corresponding to the shear vibrations between Ga and O atoms (see Figure S1 of the Supporting Information). This implies that $Pmc2_1$ phase can be transformed into a more stable phase, like $P\bar{1}$- or β-Ga_2O_3.

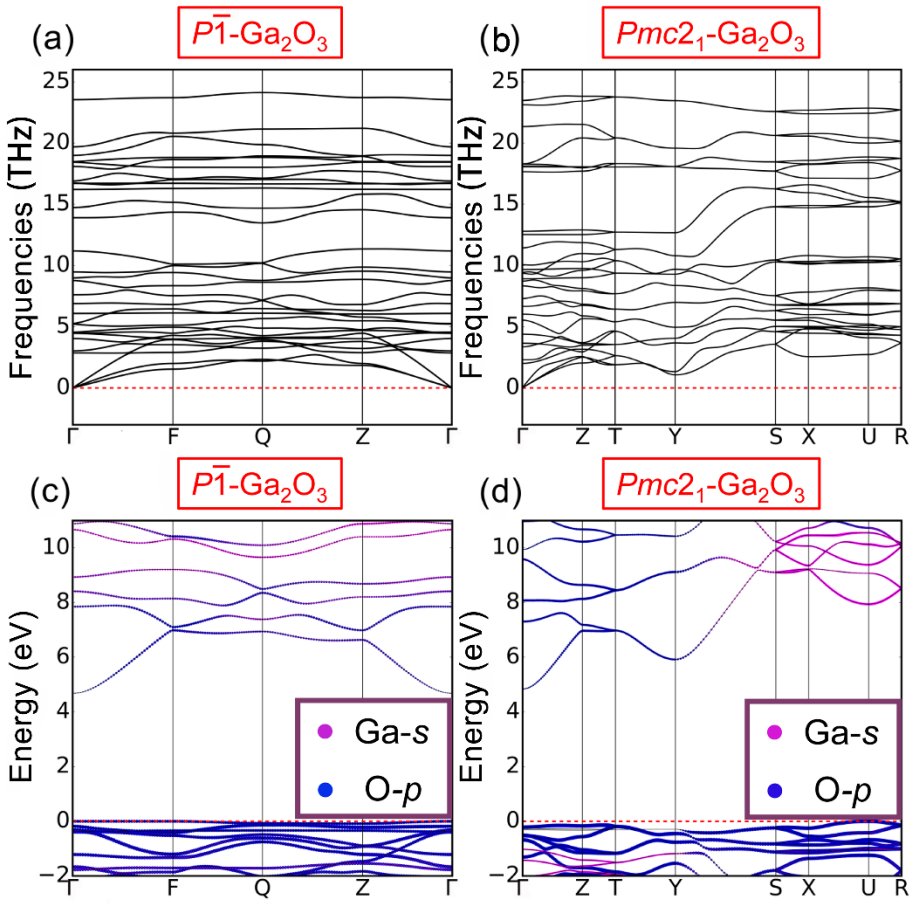

Figure 4. Calculated phonon dispersion spectrum of (a) $P\bar{1}$- and (b) $Pmc2_1$-Ga_2O_3. HSE06 calculated electronic band structure and orbital-projected density of states of (c) $P\bar{1}$- and (d) $Pmc2_1$-Ga_2O_3.

We investigated the electronic properties of $P\bar{1}$ and $Pmc2_1$ phases with HSE06 functional. The obtained band structures and orbital-projected density of states for $P\bar{1}$ and $Pmc2_1$ phases are correspondingly shown in Figure 4(c, d). The calculated band gaps of all studied Ga_2O_3 polymorphs are summarized in Figure 5(a). The β-, α-, $Pmc2_1$-Ga_2O_3 are predicted as indirect band materials with band gap values of 4.69 eV (β-Ga_2O_3), 4.98 eV (α-Ga_2O_3), 4.76 eV ($Pmc2_1$-Ga_2O_3), while κ- and $P\bar{1}$-Ga_2O_3 exhibit direct band gap character having band gaps of 4.68 eV ($P\bar{1}$-Ga_2O_3) and 4.74 eV (κ-Ga_2O_3) respectively. The calculated band gaps of α-, β- and κ-Ga_2O_3 are consistent with experiments and earlier theoretical reports.[14,48–50] The wide band gaps are particularly important for next-generation semiconducting devices operating at much higher temperatures.

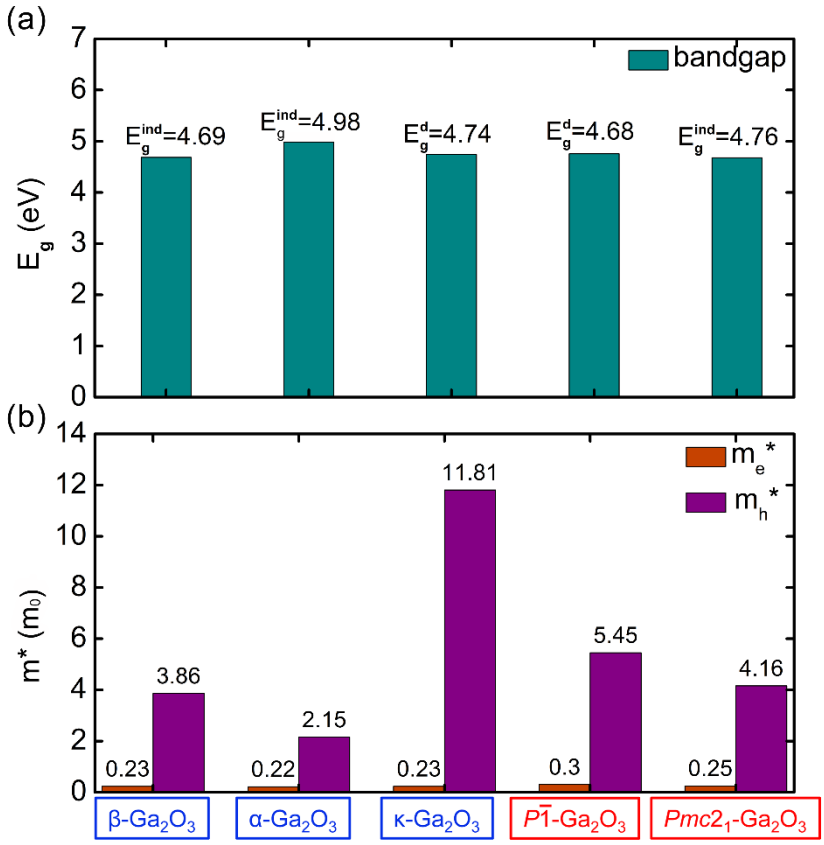

Figure 5. (a) Calculated band gaps and (b) electron and hole effective masses for β-Ga_2O_3, α-Ga_2O_3, κ-Ga_2O_3, $P\bar{1}$-Ga_2O_3, and $Pmc2_1$-Ga_2O_3.

The density of states analysis (Figure 4(c, d)) shows that the valence bands of the new phases are mainly comprised of O-*2p* orbitals. The conduction bands near the conduction band minimum (CBM) are formed due to the mixed contribution of Ga-*4s* and O-*2p* orbitals. The valence bands have a relatively weak dispersion throughout the Brillouin zone, suggesting a large effective mass for holes at the valence band maximum. The conduction band has a remarkable large dispersion due to the strong orbital hybridization between Ga and O. The calculated effective masses of electrons and holes are summarized in Figure 5(b). The results show that the hole effective masses of the selected polymorphs are about one order of magnitude larger than the electron effective mass. On the other hand, the effective masses of electrons are relativity small (0.2-0.5m_0), indicating high electron mobility. Furthermore, modification in the chemical environment of the studied Ga_2O_3 polymorphs only changes dispersions of the valence bands and not of the conduction bands.

3.3. Spontaneous Polarization of *Pmc*2$_1$-Ga_2O_3

It is generally known that ferroelectric compounds must crystallize in one of the ten polar point groups.[51] We calculated the spontaneous polarization with the Berry phase method, considering the ferroelectric κ-Ga_2O_3 for comparison. In the new phases, only *Pmc*2$_1$ phase exhibits spontaneous polarization. We built the reference structures (in space group of *Pnma* and *Pmma*) without spontaneous polarization (Figure S2 and S3 of the Supporting Information). The calculated polarizations of *Pmc*2$_1$ phase and κ-Ga_2O_3 were depicted in Figure 6. The results demonstrate that *Pmc*2$_1$-phase exhibits comparable spontaneous polarization intensity (0.277 C/m^2) as that of κ-Ga_2O_3 (0.234 C/m^2). In addition, the calculated polarization of κ-Ga_2O_3 ties well with the previously published reports.[52,53]

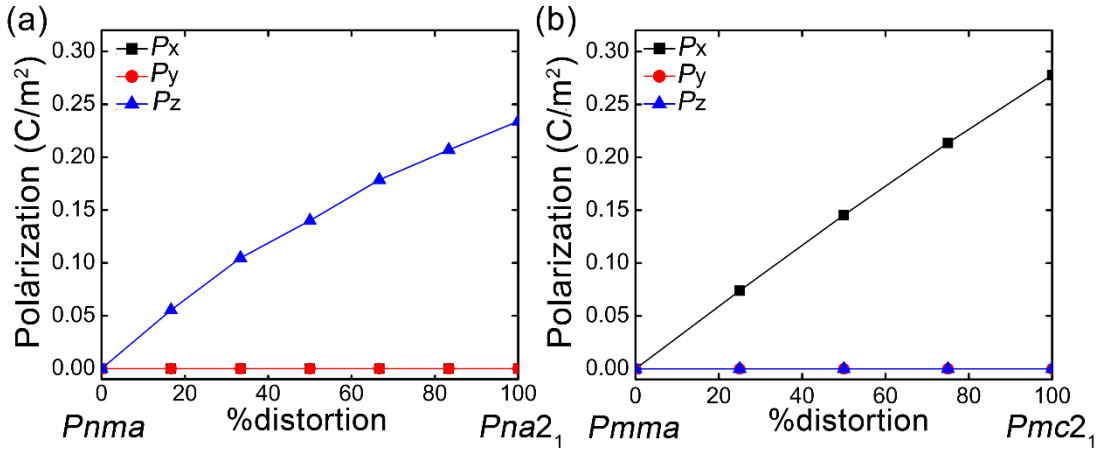

Figure 6. The calculated spontaneous polarization of (a) κ-Ga_2O_3 and (b) *Pmc*2$_1$-Ga_2O_3.

3.4. Structural Relationship of ε-Ga_2O_3 and κ-Ga_2O_3

As discussed earlier, ε-Ga_2O_3 is considered as the most stable polymorph after β-Ga_2O_3. However, in literature, several debated views exist about the crystal structure of ε-Ga_2O_3. In order to remove the disagreement between theory and experiment, we reconsidered the case of ε-Ga_2O_3 with experimentally reported hexagonal P6$_3$mc structure and carried out the structure searching using the supercell

approach. In the hexagonal structure, Ga resides at three nonequivalent sites: Ga1 with 2/3 occupancy, Ga2 with 1/3 occupancy, and Ga3 with 1/3 occupancy. Initially, we modeled 1×1×3 supercell, in which Ga1, Ga2, and Ga3 are fixed at full occupancy. Then, the Ga atoms were removed according to the corresponding occupation ratio. After complete relaxation of the structure, the result shows that the space group is *Cmc*2_1, thus confirming the results of Ref. 29. Interestingly, when we considered large size supercells (1×2×3, 1×4×3, and 1×6×3) and repeat the above steps for a total of 270 structures, we found a low energy structure with space group *Pna*2_1 containing 120 atoms (as marked by the red point in Figure 7a). In the *Cmc*2_1 phase, the tetrahedral and octahedral chains are being parallel to each other whereas, in *Pna*2_1 phase twisted wormlike chains are observed as shown in Figure 7(b, c). The *Pna*2_1 phase is found similar to that of κ-Ga_2O_3 and is further verified by the pair distribution function (PDF). The calculated g(r) of *Pna*2_1 and κ-Ga_2O_3 are almost identical in the range from 0 to 4 Å (Figure 7(d)). The above findings are in line with the previous work reported in reference 22.

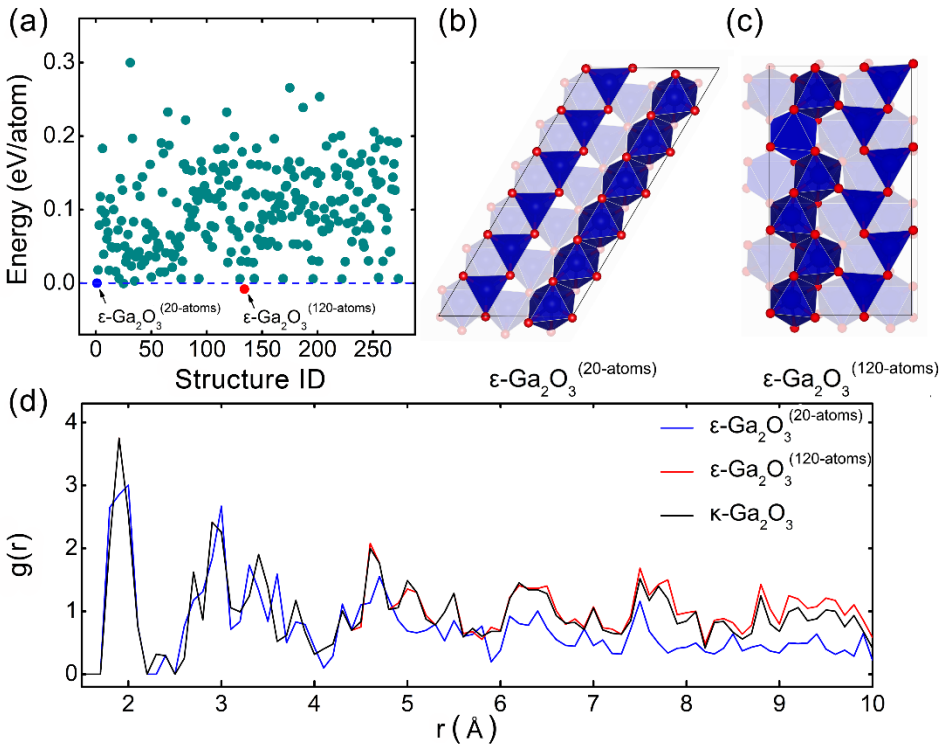

Figure 7. (a) Distribution maps of the energy difference (eV/atom) *vs* structures in established models of ε-Ga_2O_3, (b-c) The crystal structure of *Cmc*2_1 and *Pna*2_1 in [001]

projection, (d) calculated g(r) of *Cmc2*$_1$, *Pna*2$_1$, and κ-Ga_2O_3. The superscript denotes the number of atoms in the unit cell.

3.5. Structure-Property Relationship of Ga_2O_3 Polymorphs

In order to avoid duplicate statistics, we eliminated all similar structures from investigated Ga_2O_3 polymorphs fetched from the structure searches containing 2 and 8-formulas unit cells and left only ~800 structures. We then screened the structures with energy less than -4 eV/atom. Figure 8 highlights map of the PBE band gaps and averaged CNs of Ga versus energy. Although the data seems rather dispersive with no clear trend, however, the energy becomes minimum when the coordination number of Ga is averaged to ~5. The physical reason for making the structures with CNs of Ga ~ 5 the most stable ones is as follows. In group-IIIA metal oxides, such as Al_2O_3, Ga_2O_3, and In_2O_3, the structural diversity can be derived from a subtle balance between the Coulomb energy and the covalent binding energy.[54] For the Ga_2O_3 polymorphs, as more anions (O^{2-}) gather around cations (Ga^{3+}), the Coulomb energy of the system gradually increases, which is beneficial for enhancing the stability of the ionic system. On the other hand, the covalent binding energy is decreasing with the coordination number of Ga, since the electrons provided by Ga are insufficient for covalent bonding from the perspective of the local chemical environment. Because of these two competitive effects, the Ga_2O_3 polymorphs become most stable when CNs of Ga are close to a specific value (~5). This implies that the averaged CNs of Ga may be one of the descriptors of energies and band gaps in Ga_2O_3 polymorphs.

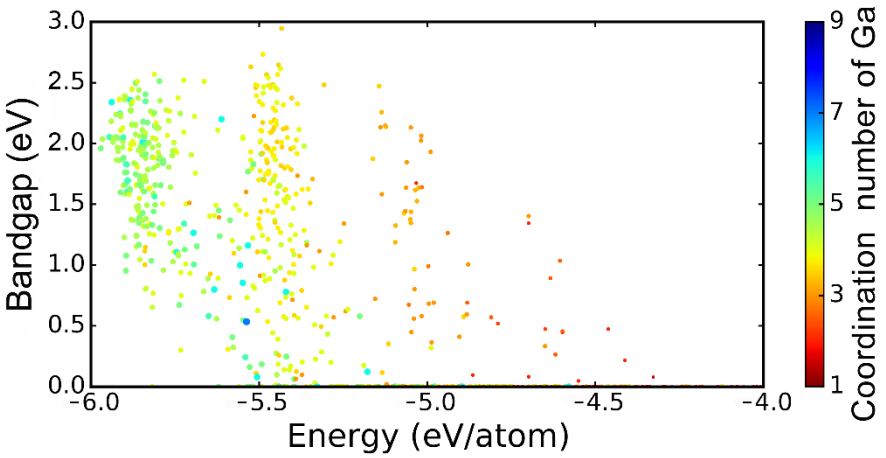

Figure 8. Distribution map of band gap and averaged coordination number of Ga versus the energy (< -4 eV/atom) for Ga_2O_3-polymorphs. The color circles depict the averaged coordination number of Ga.

4. Conclusions

We have successfully performed the structure search study of Ga_2O_3 polymorphs by employing the particle swarm optimization method in conjunction with the density functional theory calculations. We found two new energetic Ga_2O_3 polymorphs: $P\bar{1}$ and $Pmc2_1$, which needs to be confirmed and verified experimentally. The new phases exhibit significantly different XRD patterns as compared to all other known polymorphs. Specifically, we calculated lattice parameters, electronic structure, carrier effective masses, phonon dispersion spectrum, and spontaneous polarization of α-, β-, $P\bar{1}$-, $Pmc2_1$-, ε- and κ-Ga_2O_3, using different approaches. The novel phases have quite wide band gaps and small electron effective masses. The band gap values are found to span over the range of 4.6 to 4.98 eV. The $Pmc2_1$ phase exhibits electrically polar nature, with a calculated spontaneous polarization of 0.277 C/m^2, reaching that of ε/κ-Ga_2O_3. In addition, we initially explored the relationship amid energies, band gaps and CNs of Ga in Ga_2O_3 polymorphs. A primary chemical trend shows that the low energy structures have higher band gaps and averaged convergent CNs (~5) of Ga. This implies that the averaged CNs of Ga can be used as a descriptor to predict energies and band gaps in Ga_2O_3 polymorphs. Moreover, we predict that if $Pmc2_1$-Ga_2O_3 is synthesized experimentally, it may become a potential candidate for ferroelectrics.

Supporting Information

Formation enthalpies of β-, α-, κ-, $P\bar{1}$-, and $Pmc2_1$-Ga_2O_3, Lattice parameters and band gaps of α-Ga_2O_3 and β-Ga_2O_3, Lattice parameters of $P\bar{1}$ and $Pmc2_1$-Ga_2O_3, Bond length (Ga-O) of β-, κ-, α-, $P\bar{1}$-, and $Pmc2_1$-Ga_2O_3, Eigen-displacement of the lowest optical modes at Y for $Pmc2_1$-Ga_2O_3, Atomic configurations of *Pnma* and κ-Ga_2O_3, Atomic configurations of *Pmma* and $Pmc2_1$-Ga_2O_3.

Acknowledgements

L. Z. acknowledges stimulating discussions with Prof. Shibing Long (University of Science and Technology of China) and Prof. Jiangdong Ye (Nanjing University). X.W. and M.F. contributed equally to this work. This work is supported by the National Natural Science Foundation of China (Grants No. 61722403 and 11674121) and Jilin Province Science and Technology Development Program (Grant No. 20190201016JC). Calculations were performed in part at the high performance computing center of Jilin University.

References

[1] M. Östling, *Sci. China Inf. Sci.* **2011**, *54*, 1087.

[2] H. Ji, J. Zhou, M. Liang, H. Lu, M. Li, *Ultrason. Sonochem.* **2018**, *41*, 375.

[3] M. Higashiwaki, K. Sasaki, A. Kuramata, T. Masui, S. Yamakoshi, *Phys. Status Solidi A* **2014**, *211*, 21.

[4] J. Haiwei, Q. Li, Z. Lan, Z. Xinlin, Y. Rui, *MATEC Web Conf.* **2015**, *40*, 01006.

[5] S. J. Pearton, J. Yang, P. H. Cary, F. Ren, J. Kim, M. J. Tadjer, M. A. Mastro, *Appl. Phys. Rev.* **2018**, *5*, 011301.

[6] J. Millán, P. Godignon, X. Perpiñà, A. Pérez-Tomás, J. Rebollo, *IEEE Trans. Power Electron.* **2014**, *29*, 2155.

[7] H. Xue, Q. He, G. Jian, S. Long, T. Pang, M. Liu, *Nanoscale Res. Lett.* **2018**, *13*, 290.

[8] Y. Oshima, E. G. Víllora, Y. Matsushita, S. Yamamoto, K. Shimamura, *J. Appl. Phys.* **2015**, *118*, 085301.

[9] M. Higashiwaki, A. Kuramata, H. Murakami, Y. Kumagai, *J. Phys. Appl. Phys.* **2017**, *50*, 333002.

[10] S. Fujita, *Jpn. J. Appl. Phys.* **2015**, *54*, 030101.

[11] Y. Zhuo, Z. Chen, W. Tu, X. Ma, Y. Pei, G. Wang, *Appl. Surf. Sci.* **2017**, *420*, 802.

[12] Y. Kokubun, K. Miura, F. Endo, S. Nakagomi, *Appl. Phys. Lett.* **2007**, *90*, 031912.

[13] M. Higashiwaki, K. Sasaki, A. Kuramata, T. Masui, S. Yamakoshi, *Appl. Phys. Lett.* **2012**, *100*, 013504.

[14] H. H. Tippins, *Phys. Rev.* **1965**, *140*, A316.

[15] E. G. Víllora, K. Shimamura, Y. Yoshikawa, K. Aoki, N. Ichinose, *J. Cryst. Growth* **2004**, *270*, 420.

[16] H. Aida, K. Nishiguchi, H. Takeda, N. Aota, K. Sunakawa, Y. Yaguchi, *Jpn. J. Appl. Phys.* **2008**, *47*, 8506.

[17] Z. Galazka, R. Uecker, K. Irmscher, M. Albrecht, D. Klimm, M. Pietsch, M. Brützam, R. Bertram, S. Ganschow, R. Fornari, *Cryst Res Technol* **2010**, *45*, 1229.

[18] A. Kuramata, K. Koshi, S. Watanabe, Y. Yamaoka, T. Masui, S. Yamakoshi, *Jpn J Appl Phys* **2016**, *55*, 1202A2.

[19] P. Ravadgar, R.-H. Horng, S.-D. Yao, H.-Y. Lee, B.-R. Wu, S.-L. Ou, L.-W. Tu, *Optics express* **2013**, *21*, 24599.

[20] R. Zou, Z. Zhang, Q. Liu, J. Hu, L. Sang, M. Liao, W. Zhang, *Small* **2014**, *10*, 1848.

[21] M. Higashiwaki, K. Sasaki, T. Kamimura, M. Hoi Wong, D. Krishnamurthy, A. Kuramata, T. Masui, S. Yamakoshi, *Appl. Phys. Lett.* **2013**, *103*, 123511.

[22] I. Cora, F. Mezzadri, F. Boschi, M. Bosi, M. Čaplovičová, G. Calestani, I. Dódony, B. Pécz, R. Fornari, *CrystEngComm* **2017**, *19*, 1509.

[23] S. Geller, *J. Chem. Phys.* **1960**, *33*, 676.

[24] R. Roy, V. G. Hill, E. F. Osborn, *J. Am. Chem. Soc.* **1952**, *74*, 719.

[25] Ľ. Smrčok, V. Langer, J. Křesťan, *Acta Cryst.* **2006**, *63*, i83.

[26] H. Y. Playford, A. C. Hannon, E. R. Barney, R. I. Walton, *Chem. - Eur. J.* **2013**, *19*, 2803.

[27] S. Sakurai, J. Jin, K. Hashimoto, S. Ohkoshi, *J Phys Soc Jpn* **2005**, *74*, 4.

[28] B. Ollivier, R. Retoux, P. Lacorre, D. Massiotb, G. Fe´rey, *J. Mater. Chem.* **1997**, *7*, 1049.

[29] J. Kim, D. Tahara, Y. Miura, B. G. Kim, *Appl. Phys. Express* **2018**, *11*, 061101.

[30] F. Mezzadri, G. Calestani, F. Boschi, D. Delmonte, M. Bosi, R. Fornari, *Inorg. Chem.* **2016**, *55*, 12079.

[31] I. Cora, Zs. Fogarassy, R. Fornari, M. Bosi, A. Rečnik, B. Pécz, *Acta Mater.* **2020**, *183*, 216.

[32] M. Pavesi, F. Fabbri, F. Boschi, G. Piacentini, A. Baraldi, M. Bosi, E. Gombia, A. Parisini, R. Fornari, *Mater. Chem. Phys.* **2018**, *205*, 502.

[33] Y. Wang, J. Lv, L. Zhu, Y. Ma, *Comput. Phys. Commun.* **2012**, *183*, 2063.

[34] Y. Wang, J. Lv, L. Zhu, Y. Ma, *Phys. Rev. B* **2010**, *82*, 094116.

[35] P. E. Blöchl, *Phys. Rev. B* **1994**, *50*, 17953.

[36] G. Kresse, J. Furthmüller, *Phys. Rev. B* **1996**, *54*, 11169.

[37] J. P. Perdew, K. Burke, M. Ernzerhof, *Phys. Rev. Lett.* **1996**, *77*, 4.

[38] A. V. Krukau, O. A. Vydrov, A. F. Izmaylov, G. E. Scuseria, *J. Chem. Phys.* **2006**, *125*, 224106.

[39] F. P. Sabino, L. N. de Oliveira, J. L. F. Da Silva, *Phys. Rev. B* **2014**, *90*, 155206.

[40] S. Yoshioka, H. Hayashi, A. Kuwabara, F. Oba, K. Matsunaga, I. Tanaka, *J. Phys. Condens. Matter* **2007**, *19*, 346211.

[41] A. Togo, F. Oba, I. Tanaka, *Phys. Rev. B* **2008,** *78*, 134106.

[42] L. Chaput, A. Togo, I. Tanaka, G. Hug, *Phys. Rev. B* **2011**, *84*, 094302.

[43] G. K. H. Madsen, D. J. Singh, *Comput. Phys. Commun.* **2006**, *175*, 67.

[44] M. Gajdoš, K. Hummer, G. Kresse, J. Furthmüller, F. Bechstedt, *Phys. Rev. B* **2006**, *73*, 045112.

[45] D. Vanderbilt, R. D. King-Smith, *Phys. Rev. B* **1993**, *48*, 4442.

[46] Z. Liu, Y. Sun, D. J. Singh, L. Zhang, *Adv. Electron. Mater.* **2019**, *5*, 1900089.

[47] J. Lv, Y. Wang, L. Zhu, Y. Ma, *J. Chem. Phys.* **2012**, *137*, 084104.

[48] T. Ma, X. Chen, F. Ren, S. Zhu, S. Gu, R. Zhang, Y. Zheng, J. Ye, *J. Semicond.* **2019**, *40*, 012804.

[49] D. Shinohara, S. Fujita, *Jpn. J. Appl. Phys.* **2008**, *47*, 7311.

[50] H. He, R. Orlando, M. A. Blanco, R. Pandey, E. Amzallag, I. Baraille, M. Rérat, *Phys. Rev. B* **2006**, *74*, 195123.

[51] H.-Y. Ye, Y. Zhang, D.-W. Fu, R.-G. Xiong, *Angew. Chem. Int. Ed.* **2014**, *53*, 6724.

[52] K. Shimada, *Mater. Res. Express* **2018**, *5*, 036502.

[53] M. B. Maccioni, V. Fiorentini, *Appl. Phys. Express* **2016**, *9*, 041102.

[54] J. Ma, S.-H. Wei, *Comput. Mater. Sci.* **2015**, *104*, 35.

Supporting Information

Table of Contents

1. Formation enthalpies of β-, α-, κ-, $P\bar{1}$-, and $Pmc2_1$-Ga_2O_3.

Table S1. Calculated formation enthalpies ΔH (in meV/atom) of β-Ga_2O_3, α-Ga_2O_3, κ-Ga_2O_3, $P\bar{1}$-Ga_2O_3, and $Pmc2_1$-Ga_2O_3 with respect to decomposition into the elemental solids, respectively. The crystalline structures of solid phases of Ga[1] and O[2] were used for evaluating ΔH.

	β-Ga_2O_3	α-Ga_2O_3	κ-Ga_2O_3	$P\bar{1}$-Ga_2O_3	$Pmc2_1$-Ga_2O_3
ΔH (eV/atom)	-1.9243	-1.8977	-1.9049	-1.9214	-1.8990

2. Lattice parameters and band gaps of β-Ga_2O_3 and α-Ga_2O_3

Table S2. Experimental lattice parameters[3,4] and bandgaps[5,6] in comparison with the computational (this work) results for α-Ga_2O_3 and β-Ga_2O_3.

	Lattice parameters (Å) exp. [this work]			Bandgaps (eV)		
Compound	***a***	***b***	***c***	**PBE**	**HSE**	**exp.**
β-Ga_2O_3($C2/m$)	12.230	3.040	5.880	1.96	4.69	4.70
	[12.466]	[3.088]	[5.882]			
α-Ga_2O_3 ($R\bar{3}c$)	5.310	5.310	5.310	2.39	4.98	5.03
	[5.405]	[5.405]	[5.405]			

3. Lattice parameters of $P\bar{1}$-Ga_2O_3 and $Pmc2_1$-Ga_2O_3

Table S3. Calculated lattice parameters of $P\bar{1}$-Ga_2O_3 and $Pmc2_1$-Ga_2O_3.

Compound	Space group	Lattice parameters	Atomic coordinates (fractional)			
		(Å, °)	Atoms	x	y	z
$P\bar{1}$-Ga_2O_3	$P\bar{1}$	a= 3.2326	Ga	0.0140	-0.7136	-0.6855
		b= 6.0490	Ga	-0.3091	-0.2277	-0.8456
		c= 6.7259	O	-0.8578	-0.2818	-0.9969
		α= 107.7045°	O	-0.4143	-0.8932	-0.7217
		β= 103.9019°	O	-0.1283	-0.3769	-0.6285
		γ= 74.5299°				
$Pmc2_1$-Ga_2O_3	$Pmc2_1$	a= 9.1213	Ga	0.0000	0.3890	-0.1501
		b= 2.9839	Ga	-0.5000	0.1304	-0.4610
		c=4.9954	O	0.0000	0.0936	-0.0264
		α=β=γ=90°	O	0.0000	0.2707	-0.3425
			O	-0.5000	0.6010	-0.1159

4. Bond length (Ga-O) of β-, κ-, α-, $P\bar{1}$-, and *Pmc*2$_1$-Ga_2O_3

Table S4. Calculated bond lengths for β-Ga_2O_3, κ-Ga_2O_3, α-Ga_2O_3, $P\bar{1}$-Ga_2O_3 and *Pmc*2$_1$-Ga_2O_3.

	β-Ga_2O_3	α-Ga_2O_3	κ-Ga_2O_3	$P\bar{1}$-Ga_2O_3	*Pmc*2$_1$-Ga_2O_3
Average (Å)	1.966	2.031	2.013	1.919	1.896
Minimum (Å)	1.860	1.955	1.844	1.843	1.852
Maximum (Å)	2.111	2.107	2.430	2.069	1.971

5. Eigen-displacement of the lowest optical modes at Y for *Pmc*2$_1$-Ga_2O_3

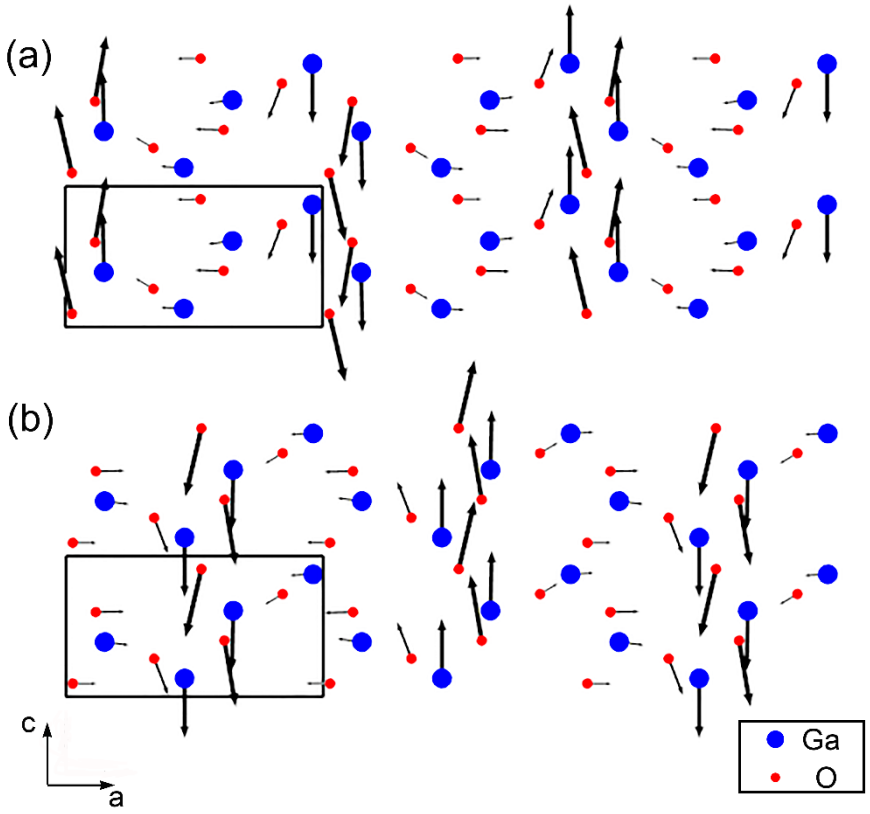

Figure S1. Calculated eigen-displacement of the lowest optical modes at Y for *Pmc*2$_1$-Ga_2O_3. The degeneracy of the lowest optical modes (1.068 THz) at Y is two. (a) 1st optical mode. (b) 2nd optical mode.

6. Atomic configurations of *Pnma* and κ-Ga_2O_3

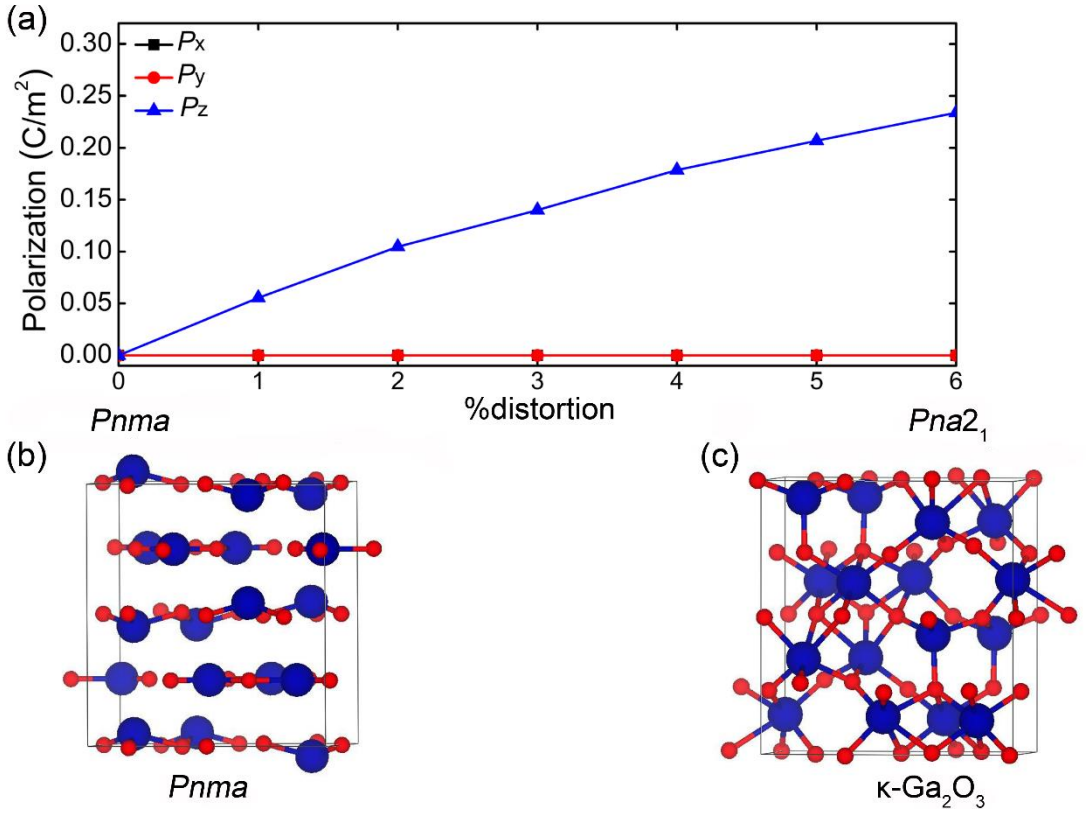

Figure S2. (a) Calculated spontaneous polarization of κ-Ga_2O_3. The atomic configurations of *Pnma* (reference structure) and κ-Ga_2O_3 are shown in (b) and (c).

7. Atomic configurations of *Pmma* and *Pmc*2$_1$-Ga_2O_3

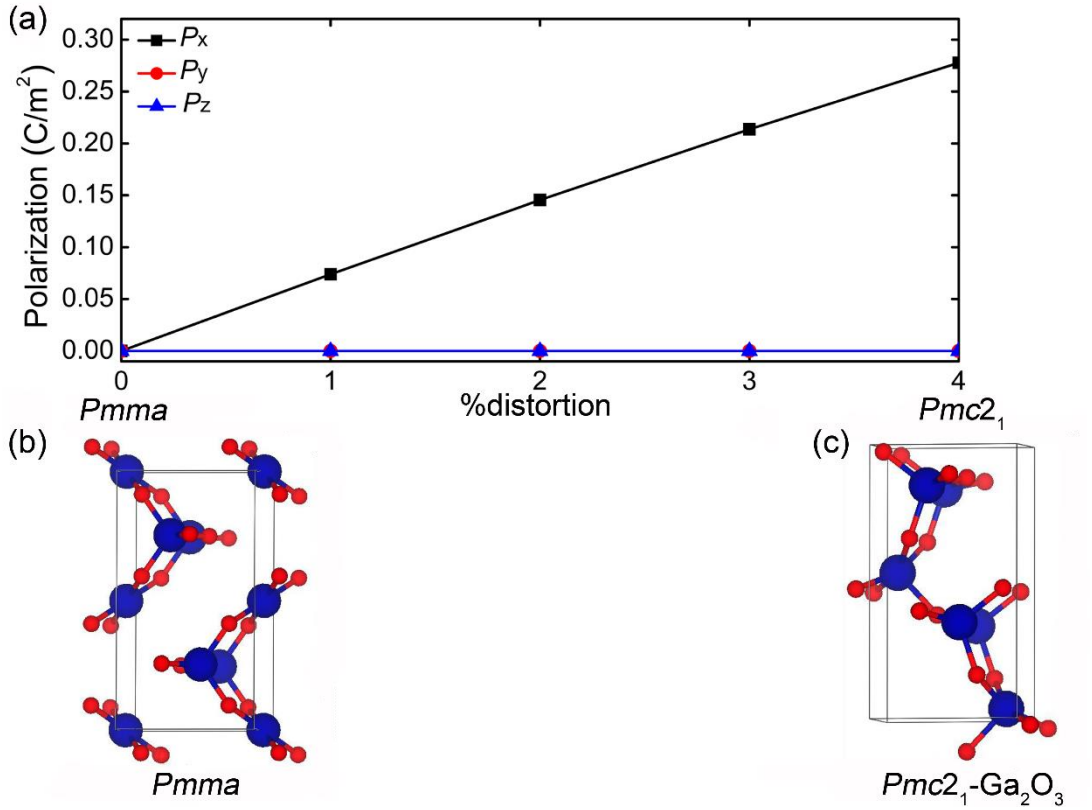

Figure S3. (a) Calculated spontaneous polarization of *Pmc*2$_1$. The atomic configurations of *Pmma* (reference structure) and *Pmc*2$_1$-Ga_2O_3 are shown in (b) and (c).

References

[1] L. Bosio, H. Curien, M. Dupont, A. Rimsky, *Acta Crystallogr. B* **1973**, *29*, 367.

[2] D. Schiferl, D. T. Cromer, R. L. Mills, *Acta Crystallogr. B* **1981**, *37*, 1329.

[3] S. Geller, *J. Chem. Phys.* **1960**, *33*, 676.

[4] G. Martínez-Criado, J. Segura-Ruiz, M.-H. Chu, R. Tucoulou, I. López, E. Nogales, B. Mendez, J. Piqueras, *Nano Lett.* **2014**, *14*, 5479.

[5] H. H. Tippins, *Phys. Rev.* **1965**, *140*, A316.

[6] T. Ma, X. Chen, F. Ren, S. Zhu, S. Gu, R. Zhang, Y. Zheng, J. Ye, *J. Semicond.* **2019**, *40*, 012804.